



Cite this: *Chem. Commun.*, 2023, 59, 6395

Received 26th February 2023,
Accepted 2nd May 2023

DOI: 10.1039/d3cc00925d

rsc.li/chemcomm

Synthesis, characterisation and multi-modal intracellular mapping of cisplatin nano-conjugates†

Aristea Anna Leventi,^{ab} Henry J. Braddick,^c Kharmen Billimoria,^b Gregory Q. Wallace,^a Heidi Goenaga-Infante,^b Nicholas C.O. Tomkinson,^{*c} Karen Faulds^{ib}*^a and Duncan Graham^{ib}*^a

The synthesis of nanocarriers for the delivery of the antitumor drug cisplatin is reported. Multimodal-imaging consisting of surface enhanced Raman scattering and laser ablation inductively coupled plasma time of flight mass spectrometry was used to visualise the intracellular uptake of both the nanocarrier and drug.

Since its approval in 1978 *cis*-diamminedichloridoplatinum(II), known as cisplatin, has been one of the leading metallodrugs prescribed for treatment of solid tumors.^{1–3} However, its clinical use is hindered by the toxic side effects^{2,4,5} and therefore the scientific focus has shifted towards finding alternatives and adopting more targeted drug delivery approaches.^{3,5}

Nanotechnology has a plethora of applications in this field, where nanoparticles (NPs) can be adopted as drug delivery vehicles promoting the preferential drug uptake in tumors compared to healthy cells.^{1,2,6,7} Various nano-based systems have been reported over the years facilitating the controlled delivery of cisplatin, such as polymeric NPs, micelles and conjugates,^{8–15} dendrimers,¹⁶ liposomes,¹⁷ nanocapsules,^{10,18} gold NPs (AuNPs),¹⁹ ferromagnetic NPs²⁰ and mesoporous silica NPs.²¹ However, to ensure successful translation of these nano-delivery systems to a clinical setting, it is vital to understand their mode of action compared to conventional chemotherapy treatments. Therefore, there is an urgent need for the tracking of these systems in complex biological environments, such as cells, to provide mechanistic insight on their uptake, drug release and action.

Surface enhanced Raman scattering (SERS) is a valuable optical imaging tool in the field of oncology, offering a high

sensitivity platform for molecular targeting with sub-cellular spatial resolution capabilities.²² As a result, SERS-active nanocarriers have been previously developed for the intracellular delivery of cisplatin.²³ However, the single-mode imaging offered by SERS can only provide limited information compared to multi-modal approaches, which compensate for the deficiencies of any single imaging modality.²⁴ Therefore, the power of SERS originates from its non-destructive nature, as it can be coupled to complementary imaging techniques. Conventional imaging modalities in cancer research include X-ray ultrasound, positron emission tomography, computed tomography or magnetic resonance imaging.^{25,26} Although each of these techniques are essential in cancer diagnostics for assessing abnormalities, they provide anatomical and/or functional information only²⁶ and lack the spatial resolution to investigate the fate of nano-based systems at a cellular level.

Herein, we demonstrate the advantages of a multi-modal imaging platform consisting of SERS and laser ablation inductively coupled plasma time-of-flight mass spectrometry (LA-ICP-ToF-MS) imaging for the intracellular visualization of cisplatin nano-conjugates (Fig. 1). The complementary nature of the two imaging techniques, which provides a combination of molecularly specific information by SERS and multi-elemental information by LA-ICP-ToF-MS, allows the detailed study of the synthesised cisplatin conjugates in cells. While SERS provides the spatial resolution to investigate single-cell uptake, LA-ICP-ToF-MS allows the fast and parallel detection of both drug and nanocarrier in multiple cells at once. Moreover, a further advantage of the coupling of these imaging modalities is the potential for quantification of the intracellular drug concentration in future studies, using SERS and an absolute quantitation model previously published by our group.²⁷ For the synthesis of cisplatin conjugates, AuNPs (a commonly adopted SERS substrate) were selected due to their non-toxic and biocompatible nature.²⁸ To ensure optimal SERS enhancement capabilities, a AuNP size of 40 nm was selected.²⁹ To provide the dual imaging traceability, the conjugates must consist of two important markers: a Raman tag that provides a strong SERS signal

^a Department of Pure and Applied Chemistry, Technology and Innovation Centre, University of Strathclyde, 99 George Street, Glasgow, G1 1RD, UK.
E-mail: duncan.graham@strath.ac.uk

^b National Measurement Laboratory, LGC, Teddington, Middlesex, TW11 0LY, UK

^c Department of Pure and Applied Chemistry, WestCHEM, Thomas Graham Building, University of Strathclyde, 295 Cathedral Street, Glasgow G1 1XL, UK

† Electronic supplementary information (ESI) available. See DOI: <https://doi.org/10.1039/d3cc00925d>



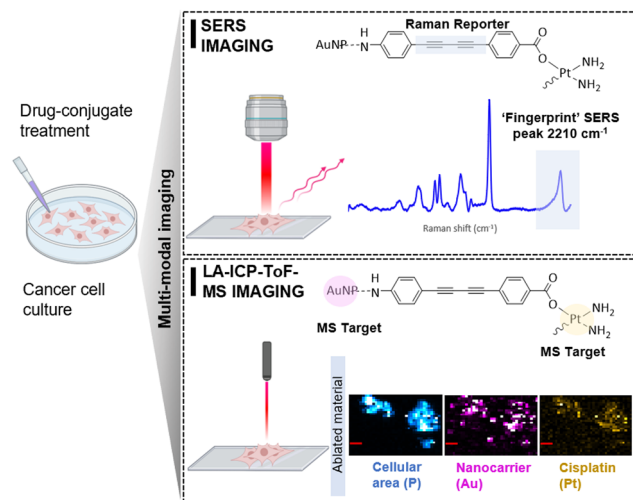


Fig. 1 Design of cisplatin conjugates demonstrating the multi-modal imaging capability for intracellular imaging.

when combined with the surface enhancing properties of the plasmonic nanostructures; and the elemental tags (Au and Pt) which are detectable by LA-ICP-ToF-MS. Therefore, the combination of these imaging modalities allows the location of both the drug and the nanoparticles to be ascertained.

The selected Raman reporter for this work was a bis-alkyne moiety (Fig. 1), as it offers the advantage of a fingerprint SERS peak (2212 cm^{-1}) within the biologically 'silent' region ($1800\text{--}2800\text{ cm}^{-1}$) that is free of background interference from cellular components.³⁰ The alkyne tag was incorporated within an organic framework, that was designed to bind both to

cisplatin and the AuNPs through a carboxylic acid and an aniline functional group respectively. Detailed protocols on the synthesis of the linker (ESI,† Fig. S1) and of the cisplatin conjugates (ESI,† Fig. S2) can be found in the supplementary information. We propose that the linker was attached to the surface of AuNPs through the aniline nitrogen, and it was experimentally observed that binding was facilitated at pH 8.5 rather than the slightly acidic pH of AuNPs as prepared (ESI,† Fig. S3). The concentration of the alkyne linker was optimized to produce a strong SERS signal without inducing colloidal instability at this stage of synthesis and was found to be $10\text{ }\mu\text{M}$ (ESI,† Fig. S4). Following the successful attachment of the linker to the AuNPs surface, the active part of cisplatin was tethered to the carboxyl terminus of the linker (Fig. 1). The drug attachment was validated by ICP-MS, where $2477 \pm 156\text{ }\mu\text{g kg}^{-1}\text{ }^{195}\text{Pt}$ was detected in the conjugate samples translating to $12.66\text{ }\mu\text{M}$ cisplatin loading in 1 mL of conjugates (ESI,† Table S1). The resulting cisplatin conjugates were characterized by extinction spectroscopy and particle tracking analysis, which revealed a monomodal character with minimal presence of aggregates and an average modal size of $47 \pm 1.7\text{ nm}$. In addition, their number-based concentration was $5.6 \pm 0.2 \times 10^{13}\text{ kg}^{-1}$ (ESI,† Fig. S5). The short-term stability of the conjugates was demonstrated with dynamic light scattering and zeta potential measurements (ESI,† Fig. S6). Furthermore, their stability was investigated in presence of RPMI media (ESI,† Fig. S7). Although the overall stability of the conjugates was moderate, the observed minor aggregation did not impact their intracellular uptake.

The dual-imaging traceability was demonstrated by introducing the conjugates to a cancerous cellular environment to better understand their mode of action. More specifically, MCF-7 breast

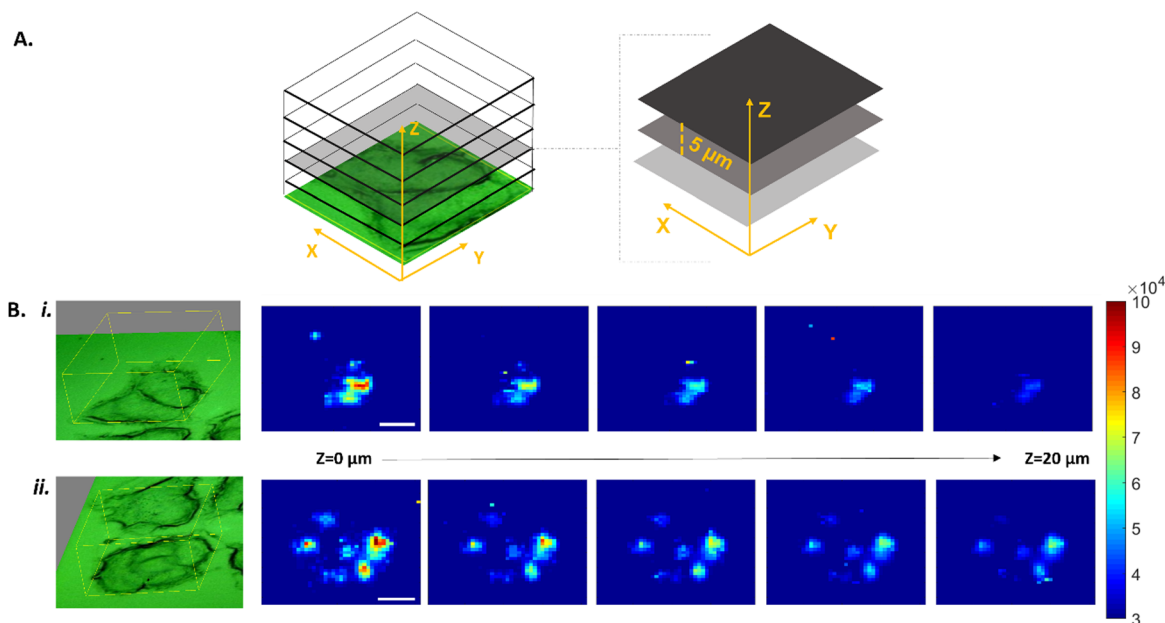


Fig. 2 3D SERS imaging of cisplatin-conjugate treated cells. A. Schematic illustration of the SERS mapping process. B. White light images of cells mapped. Subsequent false color images are for the same XY coordinates moving through the Z-plane in $5\text{ }\mu\text{m}$ steps and showing the peak area between $2155\text{--}2280\text{ cm}^{-1}$. The maps were collected with a 633 nm laser at Streamline HR high confocality mode at $1\text{ }\mu\text{m}$ resolution in the X and Y dimensions and $5\text{ }\mu\text{m}$ between Z stacks. Scale bar is $10\text{ }\mu\text{m}$.



cancer cells were cultured and treated with conjugates for 48 hours. Following treatment, the cells were fixed and spatially mapped by SERS (Fig. 2) and subsequently with LA-ICP-ToF-MS (Fig. 3). For the SERS analysis, a Renishaw InVia Raman confocal microscope equipped with a 50x/NA 0.55 N PLAN EPI objective and a HeNe 633 nm laser excitation source was used. 3D maps were collected at 1 μm resolution in the X and Y dimensions, and 5 μm between Z planes. For each sample a total of 5 Z planes were collected (20 μm range), covering a large area representing the entirety of a cell cluster (Fig. 2A). To generate the SERS maps, the total peak area between 2155–2280 cm^{-1} was determined for each collected spectrum and then reconstructed to create a false color image of the area mapped, where the high intensity pixels correspond to the presence of the alkyne peak at 2212 cm^{-1} (Fig. 2B). The fingerprint alkyne peak was observed in all Z planes of the treated cells, indicating the uptake of the cisplatin conjugates into the cells. Moreover, the high intensity pixels in the Z = 0 μm plane gradually decreased in intensity in the subsequent

planes, which suggested the internalisation of the conjugates inside the cells rather than their localisation on cell membranes. Control samples composed of citrate capped AuNPs lacking the alkyne linker did not show high intensity pixels (ESI,† Fig. S8), confirming that the observed signal originated from the alkyne and not the NP itself or the cell. To further validate the uptake of conjugates in the cancer cells, LA-ICP-ToF-MS was used for multi-elemental imaging. More specifically, the isotopes ^{31}P , ^{197}Au and ^{195}Pt were monitored, which can be assigned to the presence of cell, nanocarrier and cisplatin respectively (Fig. 3). The capability to quasi-simultaneously study multiple elements per laser pulse, can enable a detailed study of the conjugate's mode of action. Analysis of the same treated cells at a 10 μm spatial resolution showed the co-localisation of both the nanocarrier and the drug with the cells, further validating their uptake by MCF-7 cells (Fig. 3A). To demonstrate that the ^{195}Pt detection was related to the presence of cisplatin, control samples of MCF-7 cells treated with bare AuNPs were analysed and showed the absence of cisplatin (Fig. 3B).

Overall, the power of coupling the two imaging modalities was demonstrated for the investigation of the intracellular uptake of cisplatin conjugates. This imaging platform provides the spatial resolution for a detailed study of the fate of conjugates in cells, where the drug and nanoparticles can be monitored as unique species. While SERS provides the spatial resolution to study single-cell uptake, the coupling to LA-ICP-ToF-MS allows the fast and parallel detection of both drug and nanocarrier in multiple cells at once. By adopting this platform, the intracellular uptake of the conjugates was validated, with both nanoparticles and the drug being localized with the cancer cells.

In summary, the synthesis of nanocarriers for the delivery of cisplatin to cancer cells was presented. The intracellular uptake of the conjugates and the successful delivery of cisplatin to the cells were demonstrated by a multimodal imaging platform consisting of SERS and LA-ICP-ToF-MS imaging. The advantages of combining a molecularly specific, non-destructive technique like SERS with the multi-elemental imaging offered by LA-ICP-ToF-MS, can allow a detailed investigation of the intracellular fate of cisplatin. Future work will involve the quantitation of intracellular ^{197}Au and ^{195}Pt concentrations by adopting a SERS absolute quantitation model previously published by our group.²⁷ We anticipate that these conjugates will be further explored for their drug delivery effectiveness and their toxicity compared to conventional cisplatin treatments.

The data associated with this work will be available at the following link: <https://doi.org/10.15129/b8043cc3-d526-4fea-a3eb-c0027e866f3b>.

A.A.L.: conceptualisation, methodology, investigation, formal analysis, validation, visualisation, writing-original draft, writing-review and editing. H.J.B.: data curation, formal analysis, visualisation and writing-original draft. K.B.: conceptualisation, methodology, investigation, formal analysis, validation, visualisation, writing-original draft, writing-review and editing. G.Q.W.: data curation, visualisation, software. N.C.O.T.: conceptualization, methodology, resources, supervision, writing-review and editing,

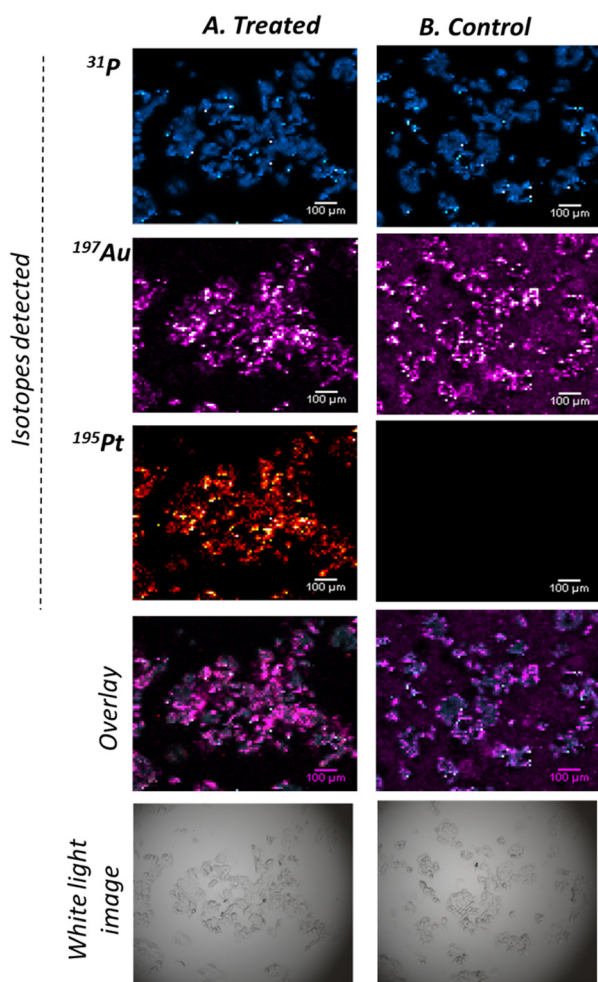


Fig. 3 LA-ICP-ToF-MS elemental maps (pixel resolution = 10 μm) of cisplatin-conjugate treated cells with corresponding light microscopy image of the cells before ablation. The ^{31}P shows the MCF-7 cells locations, ^{197}Au shows the nanocarrier and ^{195}Pt shows the cisplatin drug location. The pixel color corresponds to elemental intensity (^{31}P : 5–3000, ^{197}Au : 20–15 000 and ^{195}Pt : 5–80 counts).



funding acquisition. K.F.: conceptualization, methodology, resources, supervision, writing-review and editing, funding acquisition. D.G.: conceptualization, methodology, resources, supervision, writing-review and editing, funding acquisition.

A special thank you to Aneta Sikora and Stanislav Strekopytov for their help in the conjugate characterisation by PTA and ICPMS. Part of the work described in this manuscript was funded by the Department for Science, Innovation and Technology. We thank the University of Strathclyde for the financial support. G.Q.W. acknowledges support from the Leverhulme Trust, RPG-2020-400. Schematic illustrations created using BioRender.

Conflicts of interest

There are no conflicts to declare.

Notes and references

- 1 G. E. Craig, S. D. Brown, D. A. Lamprou, D. Graham and N. J. Wheate, *Inorg. Chem.*, 2012, **51**, 3490–3497.
- 2 X. Duan, C. He, S. J. Kron and W. Lin, *WIREs Nanomed. Nanobiotechnol.*, 2016, **8**, 776–791.
- 3 N. J. Wheate, S. Walker, G. E. Craig and R. Oun, *Dalton Trans.*, 2010, **39**, 8113–8127.
- 4 D. Kalyane, N. Raval, R. Maheshwari, V. Tambe, K. Kalia and R. K. Tekade, *Mater. Sci. Eng., C*, 2019, **98**, 1252–1276.
- 5 C. Zhang, C. Xu, X. Gao and Q. Yao, *Theranostics*, 2022, **12**, 2115–2132.
- 6 I. Brigger, C. Dubernet and P. Couvreur, *Adv. Drug Delivery Rev.*, 2002, **54**, 631–651.
- 7 E. I. Hassanen, R. M. S. Korany and A. M. Bakeer, *J. Biochem. Mol. Toxicol.*, 2021, **35**, e22722.
- 8 W. J. Rieter, K. M. Pott, K. M. L. Taylor and W. Lin, *J. Am. Chem. Soc.*, 2008, **130**, 11584–11585.
- 9 S. M. Lee, T. V. O'Halloran and S. T. Nguyen, *J. Am. Chem. Soc.*, 2010, **132**, 17130–17138.
- 10 S. Guo, L. Miao, Y. Wang and L. Huang, *J. Controlled Release*, 2014, **174**, 137–142.
- 11 S. Dhar, N. Kolishetti, S. J. Lippard and O. C. Farokhzad, *Proc. Natl. Acad. Sci. U. S. A.*, 2011, **108**, 1850–1855.
- 12 S. Dhar, Z. Liu, J. Thomale, H. Dai and S. J. Lippard, *J. Am. Chem. Soc.*, 2008, **130**, 11467–11476.
- 13 H. Uchino, Y. Matsumura, T. Negishi, F. Koizumi, T. Hayashi, T. Honda, N. Nishiyama, K. Kataoka, S. Naito and T. Kakizoe, *Br. J. Cancer*, 2005, **93**, 678–687.
- 14 K. Cheng, X.-Q. Yang, X.-S. Zhang, J. Chen, J. An, Y.-Y. Song, C. Li, Y. Xuan, R.-Y. Zhang, C.-H. Yang, X.-L. Song, Y.-D. Zhao and B. Liu, *Adv. Funct. Mater.*, 2018, **28**, 1803118.
- 15 M. Goldberg, A. Manzi, A. Birdi, B. Laporte, P. Conway, S. Cantin, V. Mishra, A. Singh, A. T. Pearson, E. R. Goldberg, S. Goldberger, B. Flaum, R. Hasina, N. R. London, G. L. Gallia, C. Bettegowda, S. Young, V. Sandulache, J. Melville, J. Shum, S. E. O'Neill, E. Aydin, A. Zhavoronkov, A. Vidal, A. Soto, M. J. Alonso, A. J. Rosenberg, M. W. Lingen, A. D'Cruz, N. Agrawal and E. Izumchenko, *Nat. Commun.*, 2022, **13**, 4829.
- 16 M. J. Pisani, N. J. Wheate, F. R. Keene, J. R. Aldrich-Wright and J. G. Collins, *J. Inorg. Biochem.*, 2009, **103**, 373–380.
- 17 H. Iinuma, K. Maruyama, K. Okinaga, K. Sasaki, T. Sekine, O. Ishida, N. Ogiwara, K. Johkura and Y. Yonemura, *Int. J. Cancer*, 2002, **99**, 130–137.
- 18 P. Sarogni, A. K. Mapanao, A. Gonnelli, M. L. Ermini, S. Marchetti, C. Kusmic, F. Paiar and V. Voliani, *iScience*, 2022, **25**, 103980.
- 19 S. D. Brown, P. Nativo, J. A. Smith, D. Stirling, P. R. Edwards, B. Venugopal, D. J. Flint, J. A. Plumb, D. Graham and N. J. Wheate, *J. Am. Chem. Soc.*, 2010, **132**, 4678–4684.
- 20 B. Thierry, F. Al-Ejeh, A. Khatri, Z. Yuan, P. J. Russell, S. Ping, M. P. Brown and P. Majewski, *Chem. Commun.*, 2009, 7348–7350.
- 21 Z. Tao, B. Toms, J. Goodisman and T. Asefa, *ACS Nano*, 2010, **4**, 789–794.
- 22 Kenry, F. Nicolson, L. Clark, S. R. Panikkanvalappil, B. Andreiuk and C. Andreou, *Nanotheranostics*, 2022, **6**, 31–49.
- 23 L. A. Austin, B. Kang and M. A. El-Sayed, *J. Am. Chem. Soc.*, 2013, **135**, 4688–4691.
- 24 M. V. Yigit, L. Zhu, M. A. Ifediba, Y. Zhang, K. Carr, A. Moore and Z. Medarova, *ACS Nano*, 2012, **5**, 1056–1066.
- 25 J. V. Jokerst and S. S. Gambhir, *Acc. Chem. Res.*, 2011, **44**, 1050–1060.
- 26 T. Beyer, L. Bidaut, J. Dickson, M. Kachelriess, F. Kiessling, R. Leitgeb, J. Ma, L. K. Shiyam Sundar, B. Theek and O. Mawlawi, *Cancer Imaging*, 2020, **20**, 38.
- 27 A. A. Leventi, K. Billimoria, D. Bartczak, S. Laing, K. Faulds, H. Goenaga-Infante and D. Graham, *Anal. Chem.*, 2023, **95**(5), 2757–2764.
- 28 M. Kus-Liškiewicz, P. Fickers and I. Tahar, *Int. J. Mol. Sci.*, 2021, **22**, 10952.
- 29 N. D. Israelsen, C. Hanson and E. Vargis, *Sci. World J.*, 2015, **2015**, 124582.
- 30 J. Wang, D. Liang, Q. Jin, J. Feng and X. Tang, *Bioconjugate Chem.*, 2020, **31**, 182–193.

